DUAL VERSUS QUADPOL: A NEW TEST STATISTIC FOR RADAR POLARIMETRY

Shane R Cloude

AEL Consultants, Regus House, Edinburgh Park, EH10 9RG, Scotland, UK, e-mail : aelc@mac.com

ABSTRACT

In this paper we develop a new statistical test to determine whether quad or dual (including compact) polarisation modes are best for use in low frequency SAR applications. We first consider a general formulation of dual/compact modes and use it to expose a fundamental weakness in compact reconstruction algorithms. We then show how all dualpol scattering problems can effectively be localised geometrically in the entropy/alpha plane. By defining a differential alpha parameter we can then establish a test statistic for determining which mode is best. We apply this test to various data sets from the ALOS-PALSAR sensor.

1. INTRODUCTION

There is currently much discussion about the relative trade-offs between dual (and compact) polarization modes versus full quad-polarimetry for use in future SAR sensors [1,2,3]. The former offer advantages of swath coverage and data rate reduction whereas the latter offers maximum flexibility in the utilization of polarization information for remote sensing applications. However, while this extra flexibility is proven useful for point scatterers [4], there remains an important question as to the need for full quadpol data in complex random scattering media such as forestry. Such media form an important class of remote sensing applications, with for example global forest biomass and stem volume being desired products for input to global climate models. All this is further complicated by dependence on sensor parameters such as wavelength, resolution, incidence angle etc.

In this paper we devise a new test statistic, applicable to all quadpol data sets, and designed to show clearly those regions where quadpol data adds value. Such tests have already been proposed using a general maximum likelihood framework and the complex Wishart distribution [5,6] but they suffer from two important drawbacks, the first is their lack of physical interpretation in terms of scattering mechanisms and the second their difficulty in dealing with singular coherency matrices, as occur often, especially in low frequency (P and L band) SAR imagery.

We overcome these two limitations by basing our test on the entropy/alpha decomposition [7,8], which gives a clear physical interpretation and secondly allows treatment of scatterers with zero entropy (singular matrices) as well as high entropy volume scatterers.

The test is based on three key ideas. The first being that for random scattering media where a two parameter dual polarization description is adequate, their H/α response lies along the lower bound of the entropy/alpha diagram (azimuthal symmetry line). We then use this to compare the observed alpha value for the pixel against a prediction based on the assumption of azimuthal symmetry. In the second stage we show that for Wishart statistics this difference has a Rayleigh distribution with an entropy dependent width parameter. We can then use this in the third and final stage to design an adaptive test statistic to determine the probability that an observed pixel contains dual or quad polarization information.

We first describe the algorithm in detail and then apply it to ALOS-PALSAR data for different forest environments to illustrate its utility and robustness in different applications.

2. DUAL AND COMPACT POLARIMETRY

We start by considering the **S** matrix represented in an arbitrary orthogonal basis **xy** used in the receiver. The fixed transmitter polarisation is then represented by complex components p_x and p_y in this basis. The key constraint of compact polarimetry is that p_x and p_y are fixed and form a unitary vector (with unit amplitude). The two orthogonal receiver channels then measure complex signals s_1 and s_2 as shown in equation 1

$$\begin{bmatrix} s_1 \\ s_2 \end{bmatrix} = \begin{bmatrix} S_{XX} & S_{XY} \\ S_{YX} & S_{YY} \end{bmatrix} \begin{bmatrix} p_x \\ p_y \end{bmatrix} \quad \text{- (1)}$$

Each of these received signals is a linear combination of the elements of [S]. The real utility of compact polarimeters lies however not in coherent analyses but in the characterisation of depolarisers. In this case interest centres not so much on the complex signals s_1 and s_2 but on their 2 x 2 coherency matrix [J] as shown in equation 2. This matrix has only four parameters, while the full scattering coherency matrix has up to sixteen. However by assuming two symmetries in the scattering process we can reduce this discrepancy. The first, reciprocity in backscatter forces $S_{xy} = S_{yx}$ and the full coherency matrix then has rank 3 with nine parameters.

Proc. of '4th Int. Workshop on Science and Applications of SAR Polarimetry and Polarimetric Interferometry – PolInSAR 2009', 26–30 January 2009, Frascati, Italy (ESA SP-668, April 2009)

$$\left.\begin{aligned} s_1 &= S_{XX}p_x + S_{XY}p_y \\ s_2 &= S_{YX}p_x + S_{YY}p_y \end{aligned}\right\} \rightarrow$$
$$[J] = \begin{bmatrix} \langle s_1 s_1^* \rangle & \langle s_1 s_2^* \rangle \\ \langle s_2 s_1^* \rangle & \langle s_2 s_2^* \rangle \end{bmatrix} = \begin{bmatrix} J_{XX} & J_{XY} \\ J_{YX} & J_{YY} \end{bmatrix} \quad \text{- (2)}$$

The second, reflection symmetry with an axis aligned parallel to x or y, forces cross products involving mixed co and crosspolar terms to zero i.e. $\langle S_{XX}S_{XY}^* \rangle = \langle S_{YY}S_{YX}^* \rangle = 0$. This reduces the scattering coherency matrix [T] and covariance matrix [C] in the **xy** basis to the reduced 3x3 forms shown in equation 3, both of which have only five unknowns.

$$[T] = \begin{bmatrix} t_{11} & t_{12} & 0 \\ t_{12}^* & t_{22} & 0 \\ 0 & 0 & t_{33} \end{bmatrix} \Leftrightarrow [C] = \begin{bmatrix} c_{11} & 0 & c_{13} \\ 0 & c_{22} & 0 \\ c_{31}^* & 0 & c_{33} \end{bmatrix} \quad (3)$$

Now we wish to relate the four observations of [J] obtained in compact polarimetry to the five unknowns of the full scattering covariance matrix under reciprocal reflection symmetry. This we can do by expanding equation 2 and using reciprocity and reflection symmetry relations to obtain the following general set of linear equations shown in equation 4.

$$\begin{bmatrix} p_x p_x^* & p_y p_y^* & 0 & 0 & 0 \\ 0 & p_x p_x^* & p_y p_y^* & 0 & 0 \\ 0 & \mathrm{Re}(p_x p_y^*) & 0 & \mathrm{Re}(p_x p_y^*) & -\mathrm{Im}(p_x p_y^*) \\ 0 & -\mathrm{Im}(p_x p_y^*) & 0 & \mathrm{Im}(p_x p_y^*) & \mathrm{Re}(p_x p_y^*) \end{bmatrix} \begin{bmatrix} c_{11} \\ c_{22} \\ c_{33} \\ \mathrm{Re}(c_{13}) \\ \mathrm{Im}(c_{13}) \end{bmatrix} = \begin{bmatrix} J_{XX} \\ J_{YY} \\ \mathrm{Re}(J_{XY}) \\ \mathrm{Im}(J_{XY}) \end{bmatrix} \Rightarrow [P]\underline{c} = \underline{j} \quad (4)$$

Here we have four equations in five unknowns and so cannot solve for all five elements of [C], whatever the choice of p_x and p_y. There are three important special cases of compact polarimetry that arise in practice. They all derive from the choice of **xy** = HV i.e. for linear horizontal and vertical on receive. In the simplest case we can then choose $p_x = 1$, $p_y = 0$ i.e. fixed horizontal transmit. In this case the [P] matrix takes the form shown in equation 5

$$p_x = 1, p_y = 0 \Rightarrow [P] = \begin{bmatrix} 1 & 0 & 0 & 0 & 0 \\ 0 & 1 & 0 & 0 & 0 \\ 0 & 0 & 0 & 0 & 0 \\ 0 & 0 & 0 & 0 & 0 \end{bmatrix} \quad \text{- (5)}$$

Here we see that [J] then only contains information about the scattered power in co and cross channels (remember that we are assuming reflection symmetry and so the HH and HV channels are uncorrelated). This for example is the case for the FBD mode of ALOS-PALSAR.

In order to access information related to the other elements a different choice of p_x and p_y are required. In the π/4 compact mode for example [1], the transmitter is set to 45 degrees linear i.e. $p_x = p_y = 1/\sqrt{2}$ and the matrix [P] takes the form shown in equation 6. We note two important aspects of this mode. The first is that we now have access to linear combinations of all the elements of [C] and hence some sensitivity to all the elements of the covariance matrix.

$$\left.\begin{aligned} p_x &= \frac{1}{\sqrt{2}} \\ p_y &= \frac{1}{\sqrt{2}} \end{aligned}\right\} \Rightarrow [P] = \frac{1}{2}\begin{bmatrix} 1 & 1 & 0 & 0 & 0 \\ 0 & 1 & 1 & 0 & 0 \\ 0 & 1 & 0 & 1 & 0 \\ 0 & 0 & 0 & 0 & 1 \end{bmatrix} \quad \text{- (6)}$$

The second is the factor of 1/2 in front of the matrix [P]. This implies a 3dB loss of signal compared to a full [S] matrix system. Such signal loss is an inevitable consequence of mismatching the transmitter and receiver bases. Finally, another mode that has been proposed is to transmit circular polarisation i.e. $p_x = 1/\sqrt{2}, p_y = \pm i/\sqrt{2}$. This case is very similar to the π/4 mode but with a [P] matrix of the form shown in equation 7

$$\left.\begin{aligned} p_x &= \frac{1}{\sqrt{2}} \\ p_y &= \frac{\pm i}{\sqrt{2}} \end{aligned}\right\}, \Rightarrow [P] = \frac{1}{2}\begin{bmatrix} 1 & 1 & 0 & 0 & 0 \\ 0 & 1 & 1 & 0 & 0 \\ 0 & 0 & 0 & 0 & \pm 1 \\ 0 & \pm 1 & 0 & \mp 1 & 0 \end{bmatrix} \quad \text{- (7)}$$

Some authors have tried to extend this approach so as to be able to reconstruct the reflection symmetric [C] matrix in full [1,3]. To do this we require an extra constraint equation between the elements of [C] so as to reduce the number of unknown to four, so matching the number of observations. Ideally we would like to find

an extra linear relationship so we could make [P] a 5x5 square matrix and then solve for the elements of $\underline{c}$ by matrix inversion. However so far no such linear relationship has been found and instead a nonlinear constraint is widely used. We can motivate the development of this approach as follows.

One way to reduce the number of unknowns in [C] is to assume a model of scattering. We adopt the widely used random-volume-over-ground or RVOG model for scattering by natural terrain [9]. In this case we assume the volume scattering component shows the much stronger azimuthal symmetry and it is only the presence of the direct surface or dihedral returns that break this symmetry and leads to a reflection symmetric composite. This model can now be used to relate the normalised level of cross-polarisation to the copolar coherence as shown in equation 8.

$$\begin{aligned}
&[T] = [T_s] + [T_V] \\
&[T_V] = \begin{bmatrix} t_{11} & 0 & 0 \\ 0 & t_{22} & 0 \\ 0 & 0 & t_{22} \end{bmatrix} \\
&\Rightarrow 4\left\langle |S_{XY}|^2 \right\rangle = \left\langle |S_{XX} - S_{YY}|^2 \right\rangle \\
&\Rightarrow \frac{\left\langle |S_{XY}|^2 \right\rangle}{\left\langle |S_{XX}|^2 \right\rangle + \left\langle |S_{YY}|^2 \right\rangle} = \frac{1}{4}(1 - |\gamma_{XXYY}|)
\end{aligned} \quad \text{- (8)}$$

Start by considering the limiting case of zero surface component i.e. pure volume scattering. In this case the coherency matrix is diagonal with two degenerate eigenvalues. This does indeed lead to an additional relationship between the cross-polarised power and the power in the second Pauli channel as shown. By expanding and using the fact that for azimuthal symmetry the copolarised powers in XX and YY are equal, we obtain a relationship between the HH/VV coherence and normalized cross-polarised power as shown in equation 8. The key assumption that has been proposed [1,3] is that this relationship applies even when we add non-zero surface components.

To check this, we first ask what happens in the limit as the volume tends to zero and we are left with bare surface scattering. In this case (according to the RVOG model) the coherency matrix is rank-1 (or with very small secondary eigenvalues) and is therefore represented by a symmetric scattering matrix, which we also assume is diagonal in the XY basis (due to Bragg scattering from a flat surface for example). Hence it has zero cross-polarisation combined with a high polarimetric coherence equal to unity. We see that this combination is still consistent with equation 8. For the general mixed case between these two extremes we can adopt a simple two-component decomposition as shown in equation 9.

$$\begin{aligned}
&[T] = [T_s] + [T_V] \\
&= m_s \begin{bmatrix} \cos^2\alpha & \sin\alpha\cos\alpha e^{i\delta} & 0 \\ \sin\alpha\cos\alpha e^{-i\delta} & \sin^2\alpha & 0 \\ 0 & 0 & 0 \end{bmatrix} \\
&+ m_v \begin{bmatrix} 0.5 & 0 & 0 \\ 0 & 0.25 & 0 \\ 0 & 0 & 0.25 \end{bmatrix}
\end{aligned} \quad \text{- (9)}$$

Here we combine two components, one a rank-1 surface mechanism with magnitude m_s and the second a random dipole cloud with scattering cross section m_v. We can now express the cross-to-copolarised scattering ratio and HH/VV coherence as functions of the surface-to-volume scattering ratio $\mu = m_s/m_v$ and scattering mechanisms α and δ as shown in equation 10.

$$\begin{aligned}
&\frac{4\left\langle |S_{HV}|^2 \right\rangle}{\left\langle |S_{HH}|^2 \right\rangle + \left\langle |S_{VV}|^2 \right\rangle} = \frac{1}{2\mu + \frac{3}{2}} \\
&1 - |\gamma_{HHVV}| = 1 - \left| \frac{\frac{1}{4} + \mu(\cos 2\alpha + i \sin 2\alpha \sin\delta)}{\sqrt{\mu^2(1 - \sin^2 2\alpha \cos^2\delta) + \frac{3}{2}\mu + \frac{9}{16}}} \right|
\end{aligned} \quad \text{- (10)}$$

We can now use this to check the equality of equation 8 for *arbitrary* mixtures of surface and volume scattering mechanisms. Figure 1 shows some example calculations.

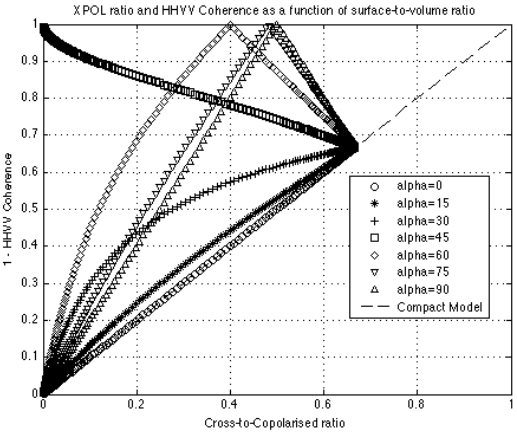

Figure 1: Test of Compact-POL Reconstruction algorithm for changing alpha parameter and varying surface-to-volume ratio

Here we plot along the x-axis the cross-to-copolar ratio and along the y-axis one-minus-the-coherence amplitude. Hence for equation 8 to be valid we require the points to lie along a line at 45 degrees. We show

how the two parameters vary for μ ranging from –30dB to +30dB i.e. from the limiting cases of zero surface to zero volume scattering. We show the results for steps of 15 degrees in alpha (always with δ = 0 to simplify the problem), starting from zero. We note that for α = 0 the equality holds for all mixtures and that the two limiting points of zero surface (the origin) and zero volume (when both approach 2/3) are also satisfied for all scattering mechanisms as expected. However for alpha angles greater than 30 degrees we note significant departures from the model. In particular for alpha = 45 degrees we see that we have a situation where the coherence can be zero even when there is low cross polarisation. This arises because one of HH or VV scattering coefficients goes to zero for this mechanism.

More significantly we see that for all alpha values greater than 45 degrees i.e. for dihedral scattering of all types, there is always a μ value that leads to zero coherence and consequently to large deviations from the simple linear relationship. We can see from equation 10 that this arises when cos2α is negative, as then it can cancel the positive numerator contribution from the volume scattering. As such this effect has its origin in the 180 degrees phase shift caused by double reflection.

From this we conclude that the simple compact-pol reconstruction algorithm in equation 8 (see [1]) is unreliable, not just for point scatterers but also for a wide range of mixed surface/volume scattering problems, even when they satisfy the reflection symmetry assumption. This is in line with other studies (see [3]) but here we have supported it analytically using RVOG rather than simply from data processing.

We further conclude that the only class of scattering problems where dual or compact-pol is fully supported over quadpol is the class of azimuthally symmetric scatterers. This is such an important distinction that we now develop a statistical test to identify such a class.

3. NEW STATISTICAL TEST

In the previous section we showed that dualpol modes are to be preferred to quadpol modes only for scattering problems which satisfy azimuthal symmetry. These then have a scattering vector that satisfies the following statistical model for single look complex data:

$$\underline{k} = \frac{1}{\sqrt{2}}\begin{bmatrix} S_{HH}+S_{VV} \\ S_{HH}-S_{VV} \\ 2S_{HV} \end{bmatrix} \Rightarrow p(\underline{k}) = \frac{1}{\pi^3 \det([T])} e^{-\underline{k}^T[T]^{-1}\underline{k}} \quad \text{- (11)}$$

where dualpol problems are characterized by a coherency matrix of the form shown in equation 12

$$[T] = [T_{dual}] = \begin{bmatrix} 1 & 0 & 0 \\ 0 & m & 0 \\ 0 & 0 & m \end{bmatrix} \quad 0 \le m \le 1 \quad \text{- (12)}$$

Several authors [5,6] have proposed maximum likelihood ratio test to identify such a condition on the coherency matrix. This test involves a ratio of determinants of [T]. However such a test has poor physical interpretation since a) the determinant is not easy to interpret physically in terms of surface and volume components and b) the determinant can go to zero for singular matrices. Singularity is especially a problem at low frequencies (L and P bands) when surface scattering is dominated by the small perturbation model, which predicts zero determinant for the coherency matrix [10].

To avoid these problems we instead develop a model based on the entropy/alpha approach [7,8]. In this regard we begin by recognizing that all azimuthally symmetric surface/volume problems lie along the lower bounding curve of the entropy/alpha diagram. Equation 13 then defines the H/α loci as a function of the single parameter m in equation 12. Figure 2 shows how these values vary from entropy of zero to 1. In this case we see that alpha is a function of entropy and is not independent.

$$H_{dual} = -\frac{1}{2m+1}\log_3\frac{1}{2m+1} - \frac{2m}{2m+1}\log_3\frac{m}{2m+1} \quad \text{- (13)}$$

$$\alpha_{dual} = \frac{m\pi}{2m+1}$$

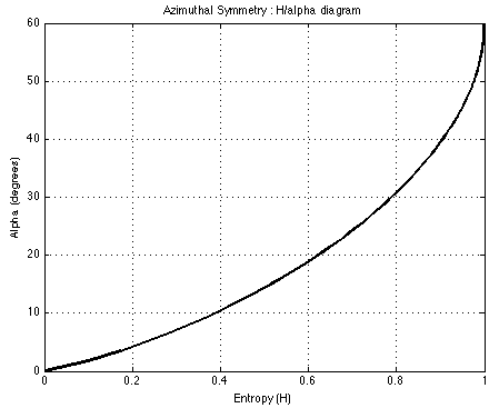

Figure 2 : Loci of entropy/alpha values for all azimuthally symmetric backscatter problems

Hence, in order to determine if a measured coherency matrix belongs to this class or not we first estimate its alpha and entropy values and then compare the alpha estimate with the prediction of alpha based on the assumption of symmetry (equation 14). This difference we then use as a test variable, as it is independent of scattering mechanism and depends only on entropy.

$$\hat{T} = \sum_{i=1}^{L} \underline{k}_i \underline{k}_i^{*T} \Rightarrow \hat{H}, \hat{\alpha} \rightarrow \Delta\alpha = \hat{\alpha} - \alpha_{dual}(\hat{H}) \quad \text{- (14)}$$

However, in order to establish a test statistic we need an idea of the probability distribution of this differential alpha as a function of two variables, firstly the equivalent number of looks (L) and secondly the entropy (H). To find this, we employed Monte-Carlo simulations of $\Delta\alpha$ for various entropies (m values) and number of looks L. To do this we used equations 11 and 12 with random number generators as shown in equation 15.

$$\underline{u} = [U][E] = \begin{bmatrix} e_1 & 0 & 0 \\ 0 & e_2 & 0 \\ 0 & 0 & e_3 \end{bmatrix}$$

$$e_i = \sqrt{\lambda_i}\{G_a(0,\tfrac{1}{2}) + iG_b(0,\tfrac{1}{2})\} \quad \text{- (15)}$$

$$[U] = \begin{bmatrix} 1 & 0 & 0 \\ 0 & 1 & 0 \\ 0 & 0 & 1 \end{bmatrix}$$

For L samples taken from Gaussian random number generators can then form an estimate of the coherency matrix as shown in equation 16

$$[\hat{T}] = \sum_{i=1}^{L} \underline{u}\underline{u}^{*T} \xrightarrow{L\to\infty} [T] \quad \text{- (16)}$$

from which we extract the statistics of $\Delta\alpha$. Figure 3 shows sample results.

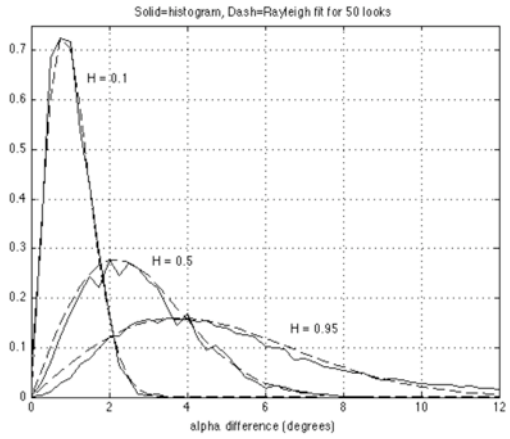

Figure 3: Distribution of differential alpha for L = 50 looks and three values of entropy

Here we show the distribution of $\Delta\alpha$ for 50 looks for three different entropy values, low (H=0.1), moderate (H = 0.5) and high (H=0.95). We see, as expected that the width of the distribution increases with entropy and also note that a Rayleigh distribution fits well (solid lines). From this we conclude that a good model for the variation of $\Delta\alpha$ is given by the probability density function shown in 17:

$$p(\Delta\alpha) = \frac{\Delta\alpha}{\sigma^2}\exp(-\frac{\Delta\alpha^2}{2\sigma^2}) \Rightarrow \overline{\Delta\alpha} = \sigma\sqrt{\frac{\pi}{2}} \quad \text{- (17)}$$

where the single parameter of the distribution σ, is defined from the mean value as shown. We can now establish a test statistic to determine if an observed $\Delta\alpha$ = x is greater than that expected from azimuthal symmetry for a given number of looks L. The idea is that if we observe x, the probability that a symmetric matrix could give a value greater than or equal to x (and hence appear non-symmetric, a false alarm) is given by (1-cdf(x)), where cdf is the cumulative distribution function for the Rayleigh distribution, given as shown in 18

$$cdf(x) = 1 - \exp(-\frac{x^2}{2\sigma(H)^2}) \quad \text{- (18)}$$

Hence the probability of x belonging to a non-symmetric matrix is just cdf(x). Hence for fixed L, we can completely characterize the fluctuations by first determining how σ varies with entropy H, i.e. $\sigma(H)$. This function we can determine using the Monte-Carlo approach for entropies ranging from 0 to 1 and for each entropy, estimating the mean. Sample results for L = 50 are shown in figure 4. The star points are numerical estimates from the Monte Caro process and the dash line is a spline fit to provide a continuous function for use in image processing. Note that a new function needs to be calculated for different number of looks L.

For a given matrix [T] we then estimate its corresponding H, $\Delta\alpha$ pair from the eigenvalues and eigenvectors, calculate $\sigma(\Delta\alpha)$ then use this value in 18 to evaluate the cdf which equals the probability that T is non-symmetric. We can then set some suitable threshold for acceptance of the symmetric hypothesis or image the probability directly as a grayscale image. In this paper we use the latter, choosing to display the probability on a scale of 0.8 (black) to 1 (white). In this way areas where quadpol is required are white whereas dualpol areas are black. We now turn to application of these ideas to data from the ALOS-PALSAR sensor.

4. APPLICATION TO ALOS-PALSAR

In this section we present results of using the Quadpol PLR21.5 mode of ALOS-PALSAR for mapping forest and vegetation cover. In particular we concentrate on applying our new test to assess the added information provided by quad-polarimetric modes (such as PLR) over simpler dual-polarisation configurations (such as

FBD). Our objective is to determine quantitative criteria useful for assessing the utility of employing such Quadpol modes in future SAR missions for land observation.

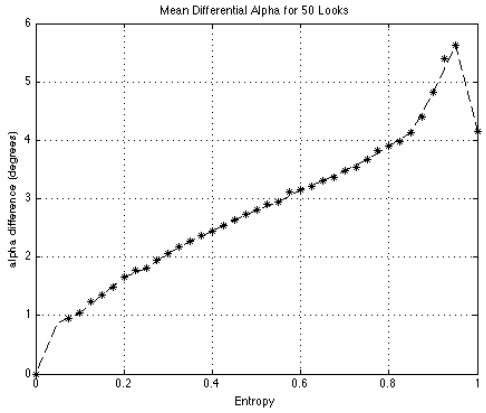

Figure 4 : Variation of width of Rayleigh distribution with entropy for L = 50 looks

To assess this, we first note that dual channel systems employ only a single polarization parameter, usually a ratio of scattered powers in co and cross-polarized channels, to characterise vegetated land cover. For PALSAR for example this is provided by the FBD mode, which employs HH and HV. The conditions under which this is a complete description of terrain scattering have been derived above and here we apply the differential alpha test to sample data sets.

We start by showing some pixel results for ocean and forest scattering. In figure 5 we show normalised eigenvalue spectra ($\sum \lambda = 1$) for the coherency matrix (100 looks) for an ocean pixel (upper) and forest pixel (lower). The ocean pixel displays surface scattering with a near singular matrix (one dominant eigenvalue). Yet its alpha value lies above the symmetric boundary and hence quadpol data still provides added information over dualpol for ocean surface scattering at L-band. In the lower portion we show a forest pixel with combined surface and volume scattering. Here we see much higher entropy. This time the alpha value lies close to the symmetric line and in this case the probability of non-symmetry is much lower, indicating that, in this case quadpol provides no added information over dualpol. We now wish to visualise this type of information over the whole image.

To visualize large data sets, we employ a colour coding for the H/alpha plane as shown in figure 6. Here colour indicates alpha from blue for surface scattering to red for dihedrals, while the saturation of colour is controlled by entropy, so low entropy has high saturation. Finally the total backscatter (trace of [T]) is used as the value for each pixel.

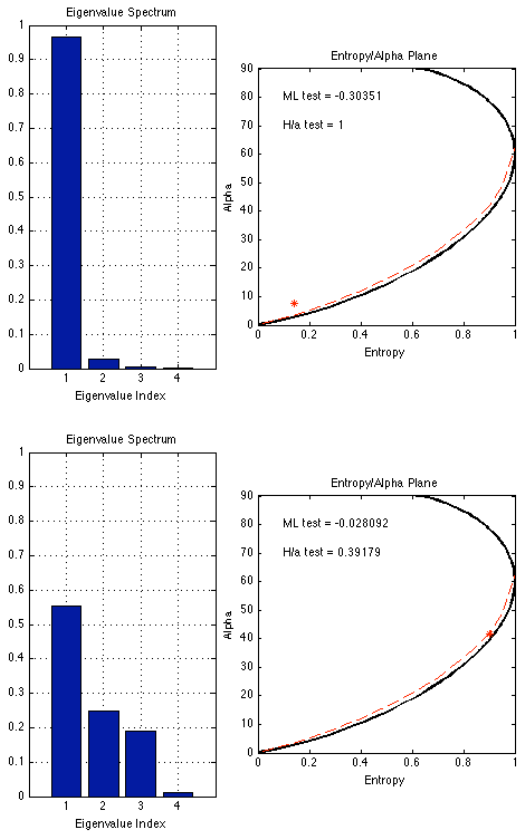

Figure 5: Normalised Eigenvalue spectra and corresponding H/a diagrams for an ocean pixel (upper) and forest pixel (lower)

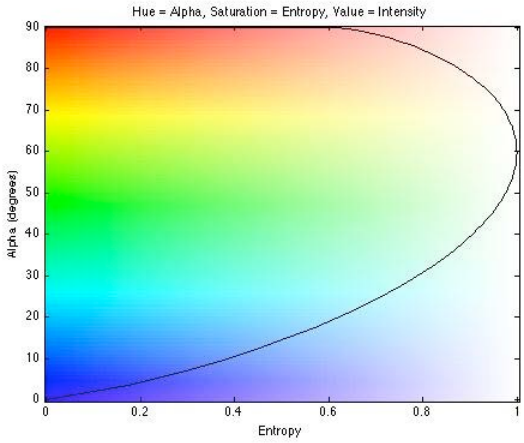

Figure 6 : Colour coding scheme used for the entropy/alpha plane

Figure 7 shows an example product for the Fife and Tayside region on the east coast of Scotland. Notice the sea surface in blue, the city of Dundee, right of centre in green and the maritime forest of Tentsmuir with low saturation in the centre.

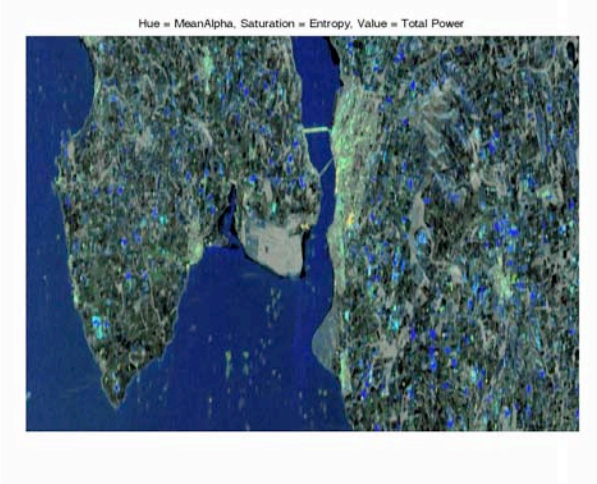

Figure 7 : Entropy/alpha HSV colour composite for Fife and Tayside region on east coast of Scotland

While we can see many different polarisation features in such images, we cannot easily see where the quad mode is adding information over dualpol. To see this we calculate the probability of non-symmetry and display it in greyscale as shown in figure 8.

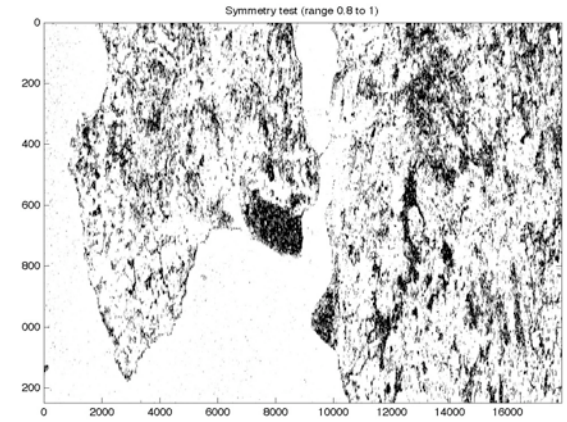

Figure 8 : Probability of non-symmetry in the range 0.8 (black) to 1(white) for the scene of figure 7 (using 100 looks)

Here we see the sea surface is white, as expected from figure 5. The agricultural areas are also white indicating the added value of quadpol. The only areas clearly black are forested (and some surface scattering like the sand dunes below the city). This result seems to indicate that forestry displays azimuthal symmetry and hence can be fully represented by just two parameters, a backscatter and one ratio (HV/HH for example).

This is such an important observation that we test it for different forest environments around the world. Figure 9 shows an HSV composite for more open Savanna woodland near Injune in Queensland, Australia Here again we can see the open surface areas in blue and the forested areas in green. This time however the quadpol mode does add information over the forests, as shown in figure 10. Here we see that the wooded areas are white and hence lie well clear of the azimuthal symmetry line.

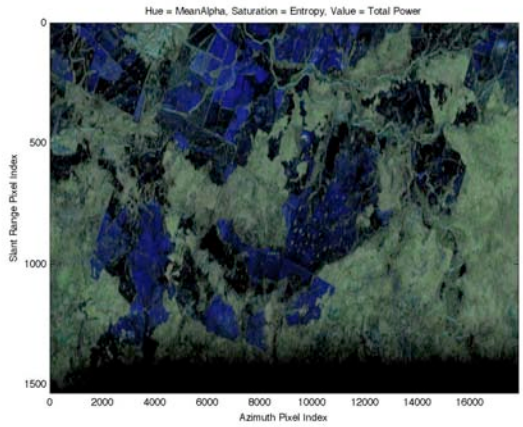

Figure 9 : Entropy/alpha HSV colour composite for Savanna woodland area near Injune, Queensland, Australia

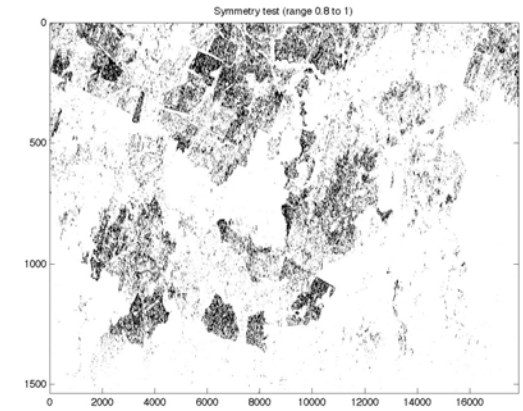

Figure 10 : Probability of non-symmetry in the range 0.8 (black) to 1(white) for the scene of figure 9 (using 100 looks)

Finally, we turn to the other extreme of a dense tropical forest environment in Belize. Figure 11 shows the entropy/alpha composite and we see an extended uniform forest area to the right of the scene. The probability image (figure 12) shows that the symmetry assumption is valid across the forested area, indicating again that quadpol in this case is not adding anything beyond dualpol.

5. CONCLUSIONS

In this paper we have developed a new statistical test to establish when quadpol modes such as PLR21.5 of ALOS-PALSAR provide additional information over dualpol modes such as FBD. We have shown how compact reconstruction algorithms are flawed, even for reflection symmetric scattering problems and how the

issue then reduces to one of identifying azimuthal symmetry in the coherency matrix.

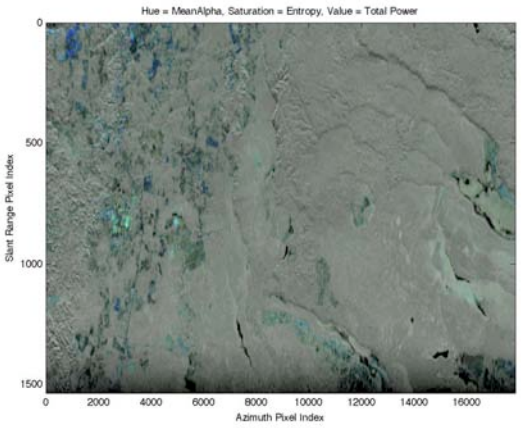

Figure 11 : Entropy/alpha HSV colour composite for tropical forest area in Belize, Caribbean

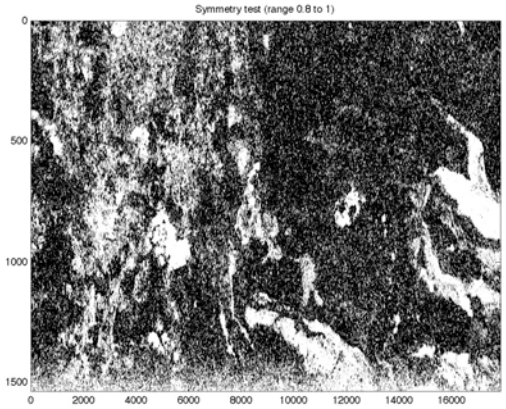

Figure 12 : Probability of non-symmetry in the range 0.8 (black) to 1(white) for the scene of figure 11 (using 100 looks)

We have applied the test to a wide range of different land-use types taken from the PALSAR global data base and have shown how quadpol is important nearly always in surface, urban and agricultural regions but also plays an important role in some forestry types. We recommend that quadpol mode design be given much higher priority that dual or compact for future SAR system, particularly at low frequencies such as L and P. Failure to do this will compromise the potential for new products development in SAR.

6. ACKNOWLDGEMENTS

We would like to acknowledge the support of JAXA for providing the PALSAR data used in this project and ESA Esrin for theirsupport under contract RFQ/3-11536/06 - POLinSAR in Orbit Demonstration.

7. REFERENCES

[1] Souyris, J-C.; Imbo, P.; Fjortoft, R.; Sandra Mingot; Jong-Sen Lee, "Compact polarimetry based on symmetry properties of geophysical media: the pi//4 mode," IEEE Transactions on Geoscience and Remote Sensing, vol.43, no.3, pp. 634-646, March 2005

[2] Raney, R.K., "Dual-polarized SAR and Stokes parameters," IEEE Geoscience and Remote Sensing Letters, vol.3, no.3, pp. 317-319, July 2006

[3] Nord M.E., T.L Ainsworth, J.S. Lee, N.J.S. Stacy, “Comparison of Compact Polarimetric Synthetic Aperture Radar Modes”, IEEE Transactions on Geoscience and Remote Sensing, accepted for publication, 2009

[4] Schneider R.Z., K. P. Papathanassiou, I. Hajnsek, A. Moreira, “Polarimetric and Interferometric Characterization of Coherent Scatterers in Urban Areas”, IEEE Transactions on Geoscience and Remote Sensing, GRS-44, pp 971-984, April 2006

[5] Ferro-Famil L., M Neumann, “Recent Advances in the Derivation of POLInSAR Statistics: Study and Applications”, Proceedings of 7th European Conference on Synthetic Aperture Radar (EUSAR), Friedrichshafen, Germany, Vol. 2, pp143-146, June 2008

[6] Conradsen, K.; Nielsen, A.A.; Schou, J.; Skriver, H.;”A test statistic in the complex Wishart distribution and its application to change detection in polarimetric SAR data”, IEEE Transactions on Geoscience and Remote Sensing, Volume 41, Issue 1, Jan. 2003 Page(s):4 – 19

[7] Cloude S.R., E. Pottier, "A Review of Target Decomposition Theorems in Radar Polarimetry", IEEE Transactions on Geoscience and Remote Sensing, Vol. 34 No. 2, pp 498-518, March 1996

[8] Cloude S.R., E. Pottier, "An Entropy Based Classification Scheme for Land Applications of Polarimetric SAR", IEEE Transactions on Geoscience and Remote Sensing, Vol. 35, No. 1, pp 68-78, January 1997

[9] Cloude S.R., K.P. Papathanassiou, “A 3-Stage Inversion Process for Polarimetric SAR Interferometry”, IEE Proceedings, Radar, Sonar and Navigation, Volume 150, Issue 03, June, pp 125-134, 2003

[10] Hajnsek I, E. Pottier, S.R. Cloude”, Inversion of Surface Parameters from Polarimetric SAR”, IEEE Transactions on Geoscience and Remote Sensing, Vol 41/4, pp 727-744, April 2003